Digital Object Identifier 10.1109/IECON.2018.8591116

IECON 2018-44th Annual Conference of the IEEE Industrial Electronics Society

Robustness analysis of voltage control strategies of smart transformer

Federico Cecati

Markus Andresen

Rongwu Zhu

Zhixiang Zou

Marco Liserre

Robustness Analysis of Voltage Control Strategies of Smart Transformer

Federico Cecati, *Student Member, IEEE*, Markus Andresen, *Member, IEEE*, Rongwu Zhu, *Member, IEEE*, Zhixiang Zou, *Member, IEEE*, Marco Liserre, *Fellow, IEEE*

Chair of Power Electronics, Christian-Albrechts-Universität zu Kiel
Kaiserstraiße 2 - 24143 Kiel, Germany
fc@tf.uni-kiel.de, ma@tf.uni-kiel.de, rzh@tf.uni-kiel.de, zz@tf.uni-kiel.de, ml@tf.uni-kiel.de

***Abstract*—The increasing penetration of Distributed Generators (DG) in the modern electric distribution network poses high priority on the problem of the stability. In this article the Harmonic Stability of a Smart Transformer-fed microgrid is investigated under different control strategies. The considered microgrid is composed by a Smart Transformer and three Distributed Generators, considering the bandwidth of the DGs unknown. The robustness is evaluated analysing the eigenvalues as a consequence of a variation of the DGs bandwidth. The system is modelled as a Multi Input Multi Output System (MIMO); the eigenvalue based analysis is carried out to assess the stability and compare the robustness of the traditional double-loop PI and a state-feedback (SF) integral controller. The results show that the SF controller ensures a higher robustness than the traditional PI controller with respect to increasing bandwidths of the DGs.**

***Index Terms*—Smart Transformer, State Space Control, Robustness**

I. Introduction

The evolution of the electric grid with the integration of distributed generators, electric vehicle charging stations and energy storage systems brings new challenges for the grid stability. The Smart Transformer (ST), which is a promising solution for the grid of the future, is a power electronic based transformer with control and communication capabilities [1]. It has the potential to integrate advanced control in order to ensure the stability, the compensation of disturbances and the optimization of the system under extremely challenging conditions. Moreover, the ST can provide low voltage DC network connectivity for the interface of DC DG and electric vehicles charging stations; that can save the costs for the infrastructures reinforcement [2].

For the ST converter control, to adopt PI in dq frame or PR in $\alpha\beta$ frame double loop controller is the standard methodology, for its simplicity and effectiveness [6]. Nevertheless, in literature other possibilities like sliding mode, deadbeat, $\mathscr{H}_\infty$ [3]–[5] have been studied. In the case that the converter is plugged into a system with a huge number of dynamics like the electric grid, the traditional PI/PR double control loop without any damping strategy may lead to critically low robustness against parameter variations, and the interaction of different grid connected converter can bring problems like harmonic instability [7], [8].

To address Harmonic Instability, at first it is necessary to investigate in which conditions it occurs, thus to state a stability condition, and afterwards to find a robust control strategy which ensures the stability also under grid parameter variations or disturbances. Impedance-based stability analysis and eigenvalue-based analysis are the two most common stability evaluation methods [7], [8].

Impedance-based stability analysis does not require a detailed system model and can assess the stability by using the ratio of the output impedance of the component to the equivalent input impedance of the series connected components [9]. However, this method is developed for Single Input Single Output (SISO) modelled system, is confined only to an interconnection point and gives only a local information about the stability [7]. Based on impedance-based condition, reshaping the converter impedance in order to satisfy the stability condition, has been proposed [11].

The advantage of the above-mentioned method is that it provides a general way to damp resonances and stabilize the grid without the need of deep information of grid model. Nevertheless, this method can introduce undesired dynamics, because of the lack of detailed model information.

The eigenvalue-based approach requires the state space model of the system and investigates the characteristics of eigenvalues and eigenvectors of state matrix to analyse the stability with a MIMO modelling [10]. Unlike the impedance-based approach, it allows a global analysis of the system, and also deeper analysis such as participation factor analysis and eigenvalue perturbation analysis [7], [10]. Building a global state space model of the system reserves several challenges: while the model of the ST is available, the model of grid is often not completely known in its structure and in its parameters.

In this article the eigenvalue-based approach is chosen for the stability analysis. Starting from the global MIMO model of the system, a full State Feedback control law (SF) is developed, in order to address Harmonic Instability. The structure of the grid is assumed to be known, and the DGs control bandwidth unknown. This bandwidth is varied along a wide range in order to study its impact on the microgrid stability through eigenvalue based analysis, both for the PI and for the SF controller.

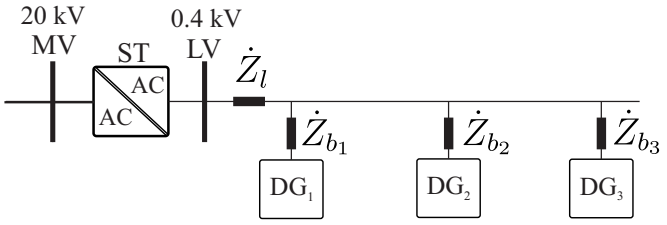

Fig. 1: Microgrid schematic: the ST is the grid forming converter and is connected to three DGs, which act as grid feeding converters.

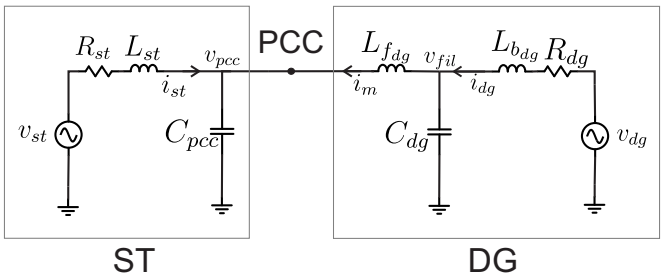

Fig. 2: Average model of a ST-fed grid with one DG connected to the PCC.

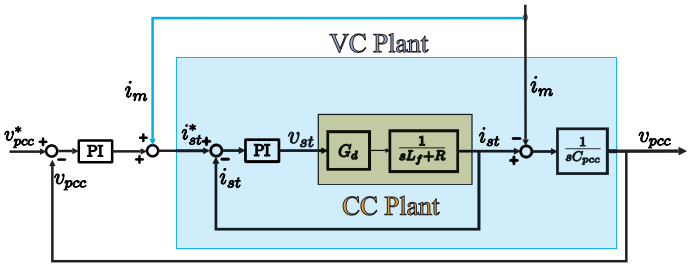

Fig. 3: Traditional PI-based double loop controller: the inner current controller plant is composed by the delay and a first order transfer function, controller through a PI. The voltage control is done through a outer PI loop with the addition of a i_{dg} feedforward term.

At first, the traditional PI double loop controller is modelled in the state space in order to realize an eigenvalue analysis under different bandwidth values. Afterwards, starting from the state space model computed for the eigenvalue analysis, a state feedback control strategy is designed and implemented, comparing its performance with the PI controller, in term of robustness against parameter variations.

The article is structured as follow: Section II describes the microgrid structure and the traditional PI double loop controller; Section III shows the control systems structures and the procedure used for the model deduction, both in the case of the PI controller and State-Feedback Integral controller. Section IV provides an analysis of the robustness respect to bandwidth variation on the DG both in the case of the PI controller and State-Feedback Integral controller; eigenvalue perturbation analysis and time domain simulation for the PCC voltage are shown to compare the control approaches. The last Section VI draws conclusions and comments about the obtained results.

II. System description and traditional double loop control

The system under consideration is shown in Fig. 1 and includes a ST with three DGs with LCL filter. The ST is modelled through an average model, as an ideal voltage source with a RL series impedance. In the control design, the converter modulations and the digital computations are modelled as a delay of $1.5T_s$ using 2^{nd} order Padè approximation, where T_s is the sampling period of the converter: the sampling frequency of the ST is 10 kHz, whereas the sampling frequency of the DG is 5 kHz.

The line impedances $\dot{Z}_b$ are modelled in series with the grid-side inductor of the DGs filter. For this reason, the value of $L_{f_{DG}}$ in Fig. 2 is the sum of the LCL filter grid-side inductance of the DG and the line inductance. Analogously, the ST output impedance includes also the line impedance $\dot{Z}_l$.

The standard control structure in the dq frame for a grid forming converter is shown in Fig. 3, and presents an inner current controller and an outer voltage controller [6]. The dynamic of the converter is approximated with a delay transfer function G_d and a RL series impedance. The current of the DG is added to the voltage controller output as a feedforward term to better compensate disturbances from the DG. For the tuning of the double loop the used technique is the Symmetrical Optimum, in order to maximize the phase margin, maintaining a good dynamic response [15].

The controller proposed in this article is based on a full State-Feedback, which exploits the informations available from the model used for the eigenvalue analysis to design the feedback law as well [12]. It includes a higher number of feedback terms, which contribute to increase the robustness under DGs parameter variations.

III. System Modelling

The representation of the system with a single DG, controlled through the traditional PI and State-Feedback Integral controller are shown in Fig. 4a and 4b respectively. It is supposed to have current sensors on each inductor branch and voltage sensors on each capacitor. Based on Fig. 2, which for simplicity of representation shows only one DG, there is the availability of the current i_{st} at the output of the ST, the voltage v_{pcc} at the PCC, the current injected by the DG i_m, the filter capacitor voltage v_{fil}, and the current at the output of the DGs i_{dg}. In the case of three DGs, the above mentioned DG variables $i_{m_{1,2,3}}$ $v_{fil_{1,2,3}}$ $i_{dg_{1,2,3}}$ are available for all the DGs. The voltage v_{dg} is regulated by a local PI current controller which tracks a current set-point i^*_{dg} provided by a Maximum Power Point Tracker (MPPT); the current set-point is considered unknown and modelled as a disturbance. The voltage v_{st} is the voltage provided by the ST, and represents the actuation variable u, while the output y in

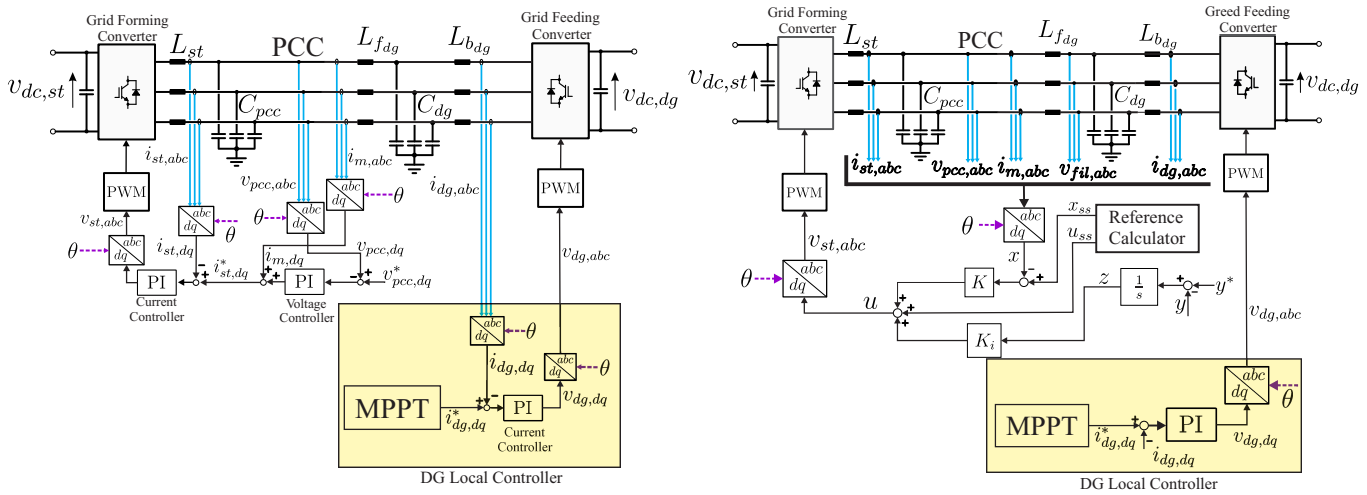

Fig. 4: Control implementation scheme in the case of a ST connected with a single DG: (a) PI controller scheme, (b) SF controller scheme

Fig. 4b is the voltage v_{pcc}, that is the variable to be controlled.

A. Converter modelling

The MIMO model of the system is realized with a modular approach in the state space and analysed with eigenvalue based approach. Both PI and SF controller are tested. The whole power system is divided into several fundamental subsystems; for each subsystem the state space model is derived. The obtained matrices of the subsystems are combined together in the overall system matrix and interconnected through proper interconnection matrices. At the beginning, the model is done for a single DG plugged to the ST, as shown in Fig. 2.

The global system can be defined in state space form as

$$\begin{cases} \dot{x} = Ax + Bu + Fi^*_{dg} \\ y = Cx + Du \end{cases} \tag{1}$$

The output y is the variable to be controller, namely v_{pcc}. The state x is defined as the concatenation of the states of each single grid component, thus $x = \left(\begin{array}{c|ccc} x_{ST} & x_{DG_1} & x_{DG_2} & x_{DG_3} \end{array} \right)^T$ where $x_{ST} = \left(\begin{array}{c|cc} d_{st} & i_{st} & v_{pcc} \end{array} \right)^T$ and $x_{DG_k} = \left(\begin{array}{cccc|c} i_{m_k} & v_{fil_k} & i_{dg_k} & z_{dg_k} & d_{dg_k} \end{array} \right)^T$ for $k = 1, 2, 3$; each voltage and current variable of the ST and DG state vector includes the d and q component, so it is a vector of dimension two. z_{dg} represent the integral of the current error, and it is used to model the PI current controller. The variables d_{st} and d_{dg_k} represent the states of the delay which approximates the power converter dynamics. They have no physical meaning, but they are fundamental to model the delay in the state space. The input u is the voltage v_{st}, the output y is the variable to be controller, namely v_{pcc}, i^*_{dg} is the vector $\left(\begin{array}{ccc} i^*_{dg_1} & \cdots & i^*_{dg_k} \end{array} \right)^T$ of the reference currents provided by the *k-th* MPPT to its DG.

The delay dynamics is derived by the canonical realization in the state space of the delay transfer function, obtaining the quadruple (A_d, B_d, C_d, D_d). Since the inputs are two, one for the d component and one for the q component, two delay systems are necessary. The resulting quadruple $(A_{DEL}, B_{DEL}, C_{DEL}, D_{DEL})$ for a dq input is defined as

$$\begin{cases} A_{DEL} = \left(\begin{array}{c|c} A_d & 0_{2x2} \\ \hline 0_{2x2} & A_d \end{array} \right) \quad B_{DEL} = \left(\begin{array}{c|c} B_d & 0_{2x1} \\ \hline 0_{2x1} & B_d \end{array} \right) \\ C_{DEL} = \left(\begin{array}{c|c} C_d & 0_{1x2} \\ \hline 0_{1x2} & C_d \end{array} \right) \quad D_{DEL} = \left(\begin{array}{c|c} D_d & 0 \\ \hline 0 & D_d \end{array} \right) \end{cases} \tag{2}$$

and the delay dynamics in the ST is given by

$$\begin{cases} \dot{d_{st}} = A_{DEL} d_{st} + B_{DEL} u \\ u_{d_{st}} = C_{DEL} d_{st} + D_{DEL} u \end{cases} \tag{3}$$

where u is the input and u_d is the delayed input; the delay model for the DGs is analogous.

The ST and the DG model are deduced through Kirchhoff laws, and the delay model is then incorporated in the matrices. For compactness of notation, the model is expressed through the following block notation: each term contained in the elements of the matrix implicitly multiplies the 2x2 identity matrix, thus is a 2x2 matrix. The dq cross coupling is expressed through a 2x2 matrix $j\omega$ defined as

$$j\omega = \begin{pmatrix} 0 & \omega \\ -\omega & 0 \end{pmatrix} \tag{4}$$

The obtained model of the ST, expressed with block notation, is

$$A'_{ST} = \begin{pmatrix} -\frac{R_{\mathrm{ST}}}{L_{\mathrm{ST}}} - j\omega & -\frac{1}{L_{\mathrm{ST}}} \\ \frac{1}{C_{\mathrm{PCC}}} & -j\omega \end{pmatrix} \tag{5}$$

$$B'_{ST} = \begin{pmatrix} \frac{1}{L_{\mathrm{ST}}} \\ 0 \end{pmatrix} \quad C'_{ST} = \begin{pmatrix} 0 & 1 \end{pmatrix} \tag{6}$$

With the same notation, that will be used from now on, the model of the DG is given by:

$$A'_{DG} = \begin{pmatrix} -j\omega & \frac{1}{L_{f\mathrm{DG}}} & 0 & 0 \\ \frac{1}{C_{\mathrm{DG}}} & -j\omega & \frac{1}{C_{\mathrm{DG}}} & 0 \\ 0 & -\frac{1}{L_{b\mathrm{DG}}} & \frac{-(R_{\mathrm{DG}}+K_p)}{L_{b\mathrm{DG}}} - j\omega & -\frac{K_i}{L_{b\mathrm{DG}}} \\ 0 & 0 & -1 & 0 \end{pmatrix} \tag{7}$$

$$F'_{DG} = \begin{pmatrix} 0 \\ 0 \\ \frac{K_p}{L_{\mathrm{DG}}} \\ 1 \end{pmatrix} \tag{8}$$

The DG model of (7) and (8) includes also the local PI controller: K_p and K_i are the proportional and integral gains. K_p determines the bandwidth of the controller, and is the parameter that is varied in the simulation to analyse the stability under different DGs bandwidth.
At these point the delay model can be incorporated in the model of the ST and the DG. Considering (3), the ST model is

$$\begin{cases} A_{ST} = \left(\begin{array}{c|c} A_{DEL} & 0_{4x4} \\ \hline B'_{ST}C_{DEL} & A'_{ST} \end{array}\right) \\ B_{ST} = \left(\begin{array}{c} B_{DEL} \\ \hline B'_{ST}D_{DEL} \end{array}\right) \\ C_{ST} = \left(\begin{array}{c|c} C'_{ST} & 0_{2\times 4} \end{array}\right) \end{cases} \tag{9}$$

The model of the DG can be deduced in the same way, considering also the PI current controller:

$$\begin{cases} A_{DG} = \left(\begin{array}{c|c} A'_{DG} & \bar{F}_{DG}C_{DEL} \\ \hline B_{DEL}G_{DG} & A_{DEL} \end{array}\right) \\ F_{DG} = \left(\begin{array}{c} \bar{F}_{DG}D_{DEL} \\ \hline B_{DEL} \end{array}\right) \end{cases} \tag{10}$$

where $\bar{F}_{DG}$ and G_{DG} are defined as

$$\bar{F}_{DG} = \begin{pmatrix} 0 & 0 & -\frac{1}{L_{\mathrm{DG}}} & 0 \end{pmatrix}^T \tag{11}$$

$$G_{DG} = \begin{pmatrix} 0 & 0 & -K_p & K_i \end{pmatrix} \tag{12}$$

The interconnection between the ST and the DGs is realized by two interconnection matrices denominated M_u and M_d, derived through Kirchhoff laws as well, that are:

$$M_d = \left(\begin{array}{cc|cc} 0 & 0 & 0 & \frac{1}{L_{f\mathrm{DG}}} \\ 0 & 0 & 0 & 0 \\ 0 & 0 & 0 & 0 \\ 0 & 0 & 0 & 0 \\ \hline 0 & 0 & 0 & 0 \\ 0 & 0 & 0 & 0 \end{array}\right) \tag{13}$$

$$M_u = \left(\begin{array}{cccc|cc} 0 & 0 & 0 & 0 & 0 & 0 \\ 0 & 0 & 0 & 0 & 0 & 0 \\ \hline 0 & 0 & 0 & 0 & 0 & 0 \\ -\frac{1}{C_{pcc}} & 0 & 0 & 0 & 0 & 0 \end{array}\right) \tag{14}$$

The overall system is realized by concatenating the models of the ST and the DGs in the diagonal of the state matrix, and using the matrices defined in (13) and (14) outside the diagonal to realize the interconnections. The model is given by (1) with:

$$A = \left(\begin{array}{c|ccc} A_{ST} & M_u & \cdots & M_u \\ \hline M_{d_1} & A_{DG_1} & \cdots & 0_{12\times 2} \\ \vdots & \vdots & \ddots & \vdots \\ M_{d_k} & 0_{12\times 2} & \cdots & A_{DG_k} \end{array}\right) \tag{15}$$

$$B = \left(\begin{array}{c} B_{ST} \\ \hline 0_{12\times 2} \\ \vdots \\ 0_{12\times 2} \end{array}\right) \tag{16}$$

$$F = \left(\begin{array}{ccc} 0_{8\times 2} & \cdots & 0_{8\times 2} \\ \hline F_{DG_1} & 0_{12\times 2} & 0_{12\times 2} \\ 0_{12\times 2} & \ddots & 0_{12\times 2} \\ 0_{12\times 2} & 0_{12\times 2} & F_{DG_k} \end{array}\right) \tag{17}$$

$$C = \left(\begin{array}{c|ccc} C_{ST} & 0_{2\times 12} & 0_{2\times 12} & 0_{2\times 12} \end{array}\right) \tag{18}$$

$$D = 0_{2\times 2} \tag{19}$$

In this paper a circuit with three DGs is used, so this model is considered with $k = 3$.

B. PI double loop modelling

In order to realize the eigenvalue perturbation analysis, the PI double loop controller must be modelled in the state space. That is done starting from Fig. 3 which shows the block diagram of the controller. The implementation of the control system on the real system is shown in Fig. 4a. The double loop can be written as

$$i^*_{ST} = \left(K_{vp}\left(v^*_{PCC} - v_{PCC}\right) + K_{vi}\int_0^t \left(v^*_{PCC} - v_{PCC}\right) d\tau\right) + i_{DG} \tag{20}$$

$$u = K_{ip}\left(i^*_{ST} - i_{ST}\right) + K_{vi}\int_0^t \left(i^*_{ST} - i_{ST}\right) d\tau \tag{21}$$

Implementing the double loop controller in the state space requires a system augmentation, which includes among the states the integral errors of the voltage and the current, namely $\int_0^t \left(v^*_{PCC} - v_{PCC}\right) d\tau$ and $\int_0^t \left(i^*_{ST} - i_{ST}\right) d\tau$. These

states will be called z_{PCC} and z_{ST} respectively; therefore the state of the ST for the PI double loop control is defined as $x_{ST_{\rm PI}} = \left(\begin{array}{cc|ccccc} d_1 & d_2 & i_{ST} & z_{ST} & v_{PCC} & z_{PCC} \end{array}\right)^T$.

The model of the ST with the addition of the integrators, without the delay is

$$A'_{ST_{\rm PI}} = \begin{pmatrix} -\frac{K_{\rm pi}+R_{\rm ST}}{L_{\rm ST}} - j\omega & \frac{K_{\rm ii}}{L_{\rm ST}} & -\frac{K_{\rm pi}\,K_{\rm pv}+1}{L_{\rm ST}} & \frac{K_{\rm iv}\,K_{\rm pi}}{L_{\rm ST}} \\ -1 & 0 & -K_{\rm pv} & K_{\rm iv} \\ \frac{1}{C_{\rm PCC}} & 0 & -j\omega & 0 \\ 0 & 0 & -1 & 0 \end{pmatrix} \tag{22}$$

$$B'_{ST_{\rm PI}} = \begin{pmatrix} \frac{K_{\rm pi}K_{\rm pv}}{L_{\rm ST}} \\ K_{\rm pv} \\ 0 \\ 1 \end{pmatrix} \tag{23}$$

By the delay inclusion the model becomes:

$$A_{ST_{\rm PI}} = \left(\begin{array}{c|c} A_{DEL} & B_{DEL}G_{ST} \\ \hline \bar{B}_{ST_{PI}}C_{DEL} & A'_{ST_{\rm PI}} \end{array}\right) \tag{24}$$

$$B_{ST_{\rm PI}} = \left(\begin{array}{c} B_{DEL} \\ \hline B'_{ST_{\rm PI}} \end{array}\right) \tag{25}$$

where

$$\bar{B}_{ST_{PI}} = \begin{pmatrix} \frac{1}{L_{\rm ST}} & 0 & 0 & 0 \end{pmatrix}^T \tag{26}$$

$$G_{ST} = \begin{pmatrix} -K_{\rm pi} & K_{\rm ii} & -K_{\rm pi}K_{\rm pv} & K_{\rm pi}K_{\rm iv} \end{pmatrix} \tag{27}$$

After deducing the model of the ST, it must be included in the whole system model through the interconnection matrices. The matrices M_d and M_u defined in (13) and (14) are not dimensionally correct for the new augmented model, and must be augmented as well. The matrix M_d is augmented with the inclusion of two columns of zeros on the left for being consistent with the dimension of the matrix $A_{ST_{\rm PI}}$, and is defined $M_{d_{\rm PI}}$. The matrix M_u, in the case of the PI double loop, includes new terms derived from the grid current feedforward, and is defined as:

$$M_{u_{\rm PI}} = \left(\begin{array}{ccccc|cc} B_{DEL}K_{\rm pi} & 0_{4x2} & 0_{4x2} & 0_{4x2} & 0_{4x2} & 0_{4x2} \\ \hline \frac{K_{\rm pi}}{L_{\rm ST}} & 0 & 0 & 0 & 0 & 0 \\ 1 & 0 & 0 & 0 & 0 & 0 \\ -\frac{1}{C_{pcc}} & 0 & 0 & 0 & 0 & 0 \\ 0 & 0 & 0 & 0 & 0 & 0 \end{array}\right) \tag{28}$$

Once the matrices $A_{ST_{\rm PI}}$, $M_{d_{\rm PI}}$ and $M_{u_{\rm PI}}$ are defined, the whole system model, with the inclusion of the ST PI double loop, can be written with in a form analogous to (19) as

$$A_{\rm PI} = \left(\begin{array}{c|ccc} A_{ST_{\rm PI}} & M_{u_{\rm PI}} & \cdots & M_{u_{\rm PI}} \\ \hline M_{d_{\rm PI_1}} & A_{DG_1} & \cdots & 0_{12\times 12} \\ \vdots & \vdots & \ddots & \vdots \\ M_{d_{\rm PI_k}} & 0_{12\times 12} & \cdots & A_{DG_k} \end{array}\right) \tag{29}$$

which can be used for the eigenvalue perturbation analysis.

C. State-Feedback Integral controller modelling

The state space form of the system, built initially for the eigenvalue based stability analysis, is particularly suitable for the application of a full State-Feedback controller. In fact, once having the state space model, the design of a State-Feedback controller can be done through eigenvalue placement or optimal control techniques. The schematic of implementation of the controller on the whole scheme is shown in Fig. 4b.

The proposed control law has the form:

$$\begin{cases} \dot{z} = y - y_{ref} \\ u = \begin{pmatrix} K & K_i \end{pmatrix} \begin{pmatrix} (\hat{x} - x_{ss}) \\ z \end{pmatrix} + u_{ss} \end{cases} \tag{30}$$

where three fundamental parts can be identified.

1) Steady-state reference calculator: The objective of this block is to compute x_{ss} and u_{ss} that are the steady-state state and input respectively to track the given reference y_{ref}. This is done by considering x_{ss} and u_{ss} linear function of the reference, so $x_{ss} = N_x y_{ref}$ and $u_{ss} = N_u y_{ref}$.

The computation of the matrices N_x and N_u can be done by the solution of the linear system.

$$\begin{pmatrix} A & B \\ C & D \end{pmatrix} \begin{pmatrix} N_x \\ N_u \end{pmatrix} = \begin{pmatrix} 0_{nx1} \\ 1_{mx1} \end{pmatrix} \tag{31}$$

2) Integrator: The integrator is composed by the first order linear differential equation $\dot{z} = y - y_{ref}$, that has as solution

$$z = \int_0^t (y(\tau) - y_{ref})\ d\tau \tag{32}$$

3) State-Feedback Integral controller: The State-Feedback Integral controller is described by equation (30), composed by an integrator for the tracking error and a feedback law composed from a state feedback, an integral feedback, and the steady-state input term. The gain matrix $\begin{pmatrix} K & K_i \end{pmatrix}$ is computed by solving the eigenvalue placement problem with the system

$$\begin{pmatrix} \dot{x} \\ \dot{z} \end{pmatrix} = \begin{pmatrix} A & O \\ -C & O \end{pmatrix} \begin{pmatrix} x \\ z \end{pmatrix} + \begin{pmatrix} B \\ -D \end{pmatrix} u \tag{33}$$

IV. Robustness evaluation

The stability analysis is realized simulating the system with different DGs controller bandwidths. The eigenvalue analysis are shown in Fig. 5 and point out the motion of the eigenvalues under the increase of the DGs bandwidth, for the PI and the SF. The simulated DG bandwidth range goes from 581 Hz to 1040 Hz. The arrow direction indicates increasing bandwidths. A time domain simulations to confirm the result of eigenvalue analysis is done in the dq frame, shown in figure. The d component of the PCC reference voltage is initially posed to 100V; at time 0.3s the voltage d component reference steps to 150V and figure 6 shows the dq time domain simulation during the voltage step, for the PI and the SF respectively.

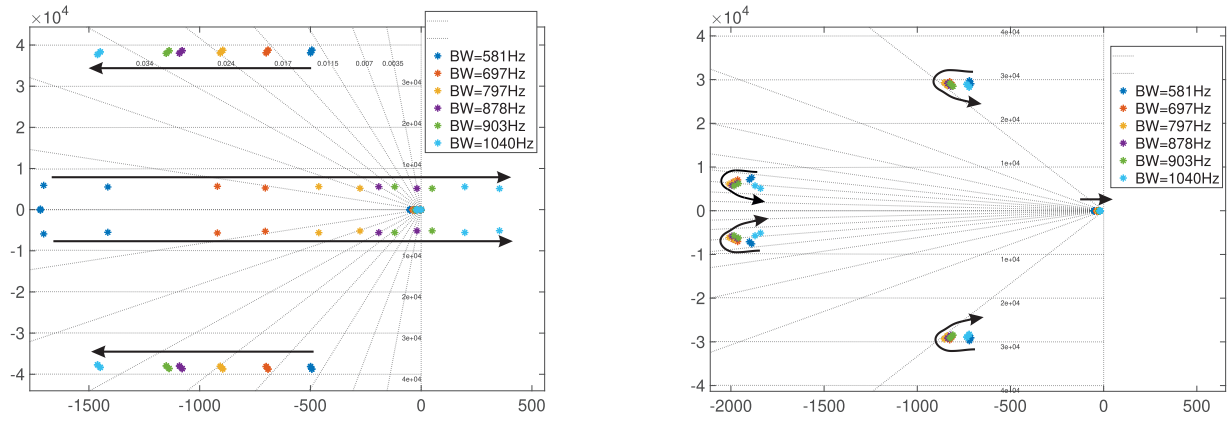

(a) (b)

Fig. 5: Eigenvalue perturbation analysis for different bandwidths: (a) PI double loop controller, (b) State-Feedback Integral controller.

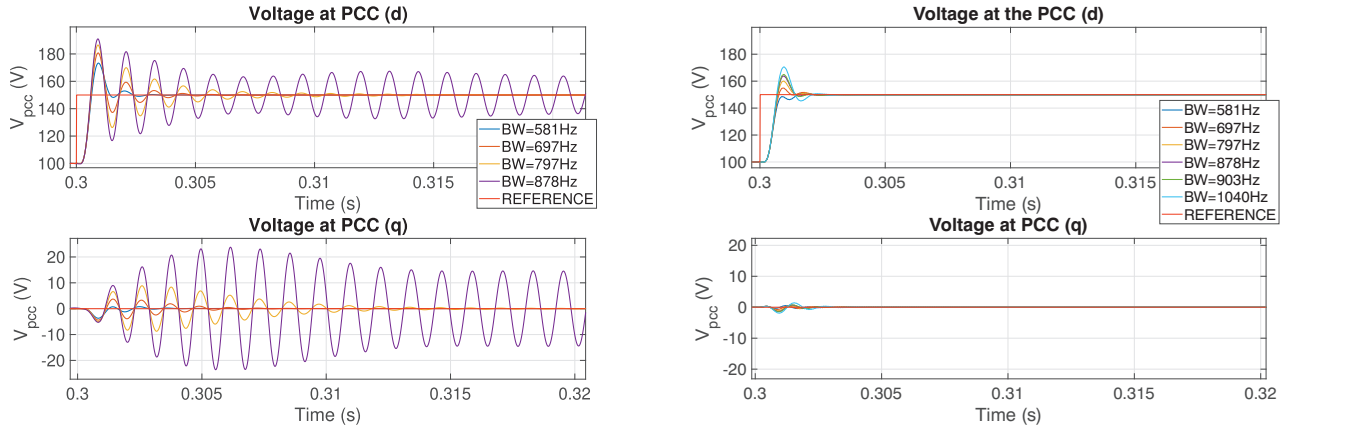

(a) (b)

Fig. 6: PCC voltage time domain simulations in the *dq* frame for different bandwidths: (a) PI double loop controller, (b) State-Feedback Integral controller.

A. PI controller robustness

The eigenvalue perturbation analysis for the PI double loop controller can be observed in Fig. 5a. On the one hand, increasing the bandwidth brings a faster response in the voltage at the PCC, which is denoted by the left shift of a group of eigenvalues. On the other hand, the increase of bandwidth brings to instability and resonance phenomena, which are denoted by the right shift of the other eigenvalues. The maximum tested stable bandwidth is 878 Hz. Fig. 6a shows the time domain simulation only for the stable bandwidths; it can be noticed that for eigenvalues closer to the imaginary axis, the oscillations becomes bigger. The bandwidths bigger than the maximum stable bandwidth are not shown in Fig. 6a because they are not stable.

B. SF controller robustness

The SF controller differs from the PI double loop for providing a full state feedback. Moreover, it includes also integral actions which ensures a performant voltage tracking and increases the robustness. The tuning methods available for the State-Feedback Integral controller are several: in these paper a LQ tracking controller has been used. The weight matrices have been chosen according to [18] in order to obtain a rising time comparable to the case of PI double loop. Fig. 5b shows the eigenvalue map done with the same bandwidth values simulated in the PI case. It can be noticed that, with respect to the PI, the robustness is much higher, and the system is stable with high margin also in the cases in which the PI is not. The poles close to the imaginary axis, that are present both in the PI case in Fig. 5a and in the SF case in Fig. 5b are not dangerous for the stability. (c) The time domain simulation in Fig. 6b confirms the high robustness of the controller which achieves a fast tracking with a modest overshoot and no persistent oscillations also with high bandwidth values.

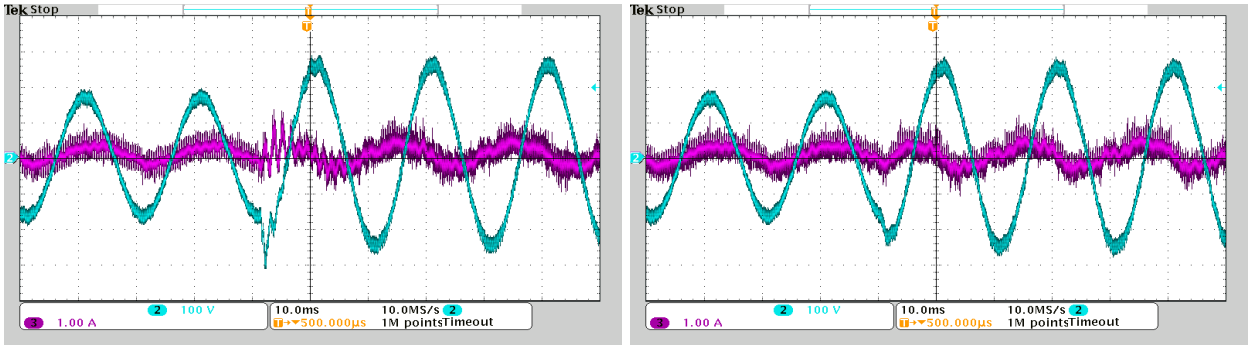

(a) (b)

Fig. 8: Experimental results of the controller response to a PCC voltage step from 100V to 150V with a DG bandwidth of 797 Hz: (a) PI double loop controller, (b) State-Feedback Integral controller.

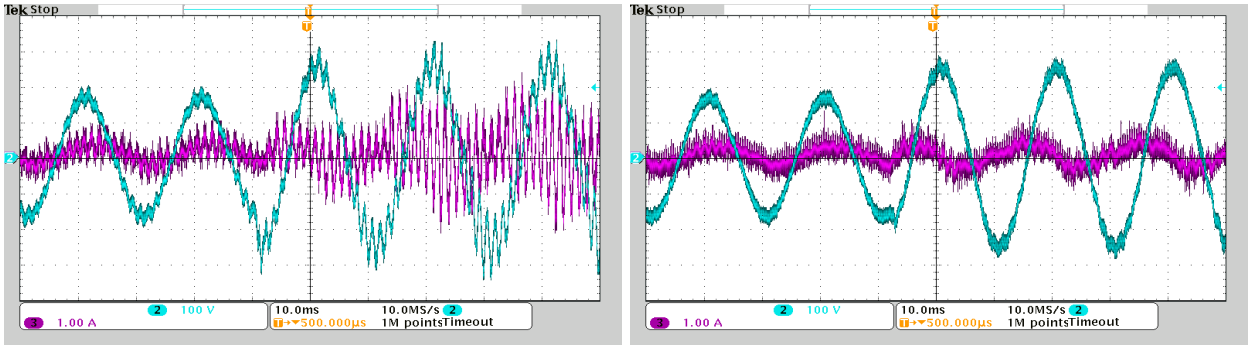

(a) (b)

Fig. 9: Experimental results of the controller response to a PCC voltage step from 100V to 150V with a DG bandwidth of 886 Hz: (a) PI double loop controller, (b) State-Feedback Integral controller.

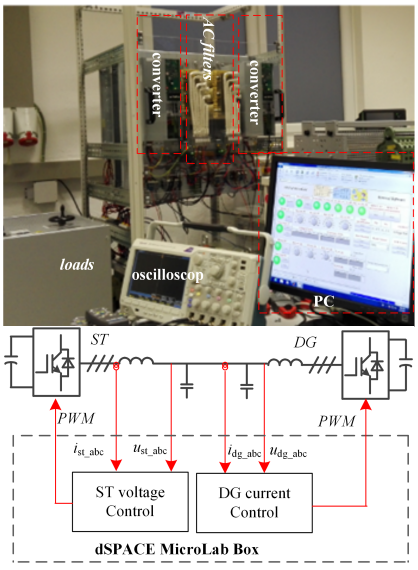

Fig. 7: Photograph and system structure of the Setup.

V. Experimental result

In this section the experimental results of the system with a high DGs bandwidth are shown. A MicroLabBox-based 15kW setup including a ST and DGs has been built in the laboratory to validate the aforementioned analysis, and is shown in Fig. 7. The switching frequency is 5 kHz for ST and 5 kHz for the DG. In AC side of ST and DG, a LC filter with 1.6 mH inductance and 5 μF capacitance is used.

The tests, shown in Fig. 8 and 9, have been done with an initial voltage at the PCC of 100V, which steps to 150V. The current injected from the DG is set to 2A. At the PCC it is plugged a resistive load of 50Ω.

The first tested bandwidth for the DG controller is 797 Hz and the experimental results are shown in Fig. 8. The obtained result is the same of the one obtained in the computer simulations reported in Fig. 6. The controller is stable in both cases, but at the moment of the voltage step it presents a most severe voltage spike and bigger oscillations in the case of PI.

The second tested bandwidth is 886 Hz shown in Fig. 9. As in the computer simulation, the PI controller is unstable under this bandwidth, while the SF controller is stable without significant oscillations.

VI. Conclusions

The simulations analyse the impact of the DGs bandwidth variations on the system stability, comparing the traditional PI double loop with the SF controller. It is observed that the

bandwidth of the DGs is a parameter of crucial importance for the system stability. In the case of the PI controller, by increasing the DGs bandwidth, the interaction of ST and DGs introduces a resonance phenomenon, which drives the system through harmonic instability. The SF controller, thanks to the feedback terms from the DGs, provides a better decoupling between the ST and the DGs dynamics, and reduce significantly the influence of DGs bandwidths on the system stability and transient response.

In the case of the PI controller, DGs unknown bandwidth variations result in a significant change of the eigenvalue configuration in the global system. A bandwidth of 797 Hz is tested at first. The voltage and the current of the Smart Transformer present a spike and a slightly damped high frequency resonance after the reference voltage step. With a DG bandwidth of 886 Hz, the Smart Transformer voltage and current present an undamped high frequency oscillation that turn to harmonic instability at the moment of the voltage step.

In the case of the SF controller, unknown DGs parameter variation are reflected in the eigenvalue configuration to a minimum extent. The experimental results confirm the theoretical ones, and demonstrate that both with a bandwidth of 797 Hz and 866 Hz, the voltage and current spikes are modest and no oscillatory phenomena appear during and after the voltage step.

ACKNOWLEDGEMENT

The authors gratefully acknowledge funding by the European Research Council under the European Union's Seventh Framework Programme (FP/2007-2013)/ERC Grant Agreement 616344 "HEART - the Highly Efficient And Reliable smart Transformer", by German Federal Ministry for Economic Affairs and Energy within the research project "Add-On" (0350022B) and by Gesellschaft für Energie und Klimaschutz Schleswig-Holstein GmbH (EKSH) doctoral studies grant.

REFERENCES

[1] M. Liserre, G. Buticchi, M. Andresen, G. De Carne, L. F. Costa and Z. X. Zou, "The Smart Transformer: Impact on the Electric Grid and Technology Challenges," in IEEE Industrial Electronics Magazine, vol. 10, no. 2, pp. 46-58, June 2016.

[2] SP ENERGY NETWORK: LV engine, https://www.spenergynetworks.co.uk/pages/lv_engine.aspx

[3] Shih-Liang Jung and Ying-Yu Tzou, "Discrete sliding-mode control of a PWM inverter for sinusoidal output waveform synthesis with optimal sliding curve," IEEE Transactions on Power Electronics, vol. 11, no. 4, pp. 567-577, Jul 1996.

[4] Q. C. Zhong, J. Liang, G. Weiss, C. M. Feng and T. C. Green, $\mathscr{H}_\infty$ Control of the Neutral Point in Four-Wire Three-Phase DC–AC Converters," IEEE Transactions on Industrial Electronics, vol. 53, no. 5, pp. 1594-1602, Oct. 2006.

[5] K. P. Gokhale, A. Kawamura and R. G. Hoft, "Dead Beat Microprocessor Control of PWM Inverter for Sinusoidal Output Waveform Synthesis," IEEE Transactions on Industry Applications, vol. IA-23, no. 5, pp. 901-910, Sept. 1987.

[6] Poh Chiang Loh, M. J. Newman, D. N. Zmood and D. G. Holmes, "A comparative analysis of multiloop voltage regulation strategies for single and three-phase UPS systems," in IEEE Transactions on Power Electronics, vol. 18, no. 5, pp. 1176-1185, Sept. 2003.

[7] M. K. Bakhshizadeh et al., "The Application of Vector Fitting to Eigenvalue-Based Harmonic Stability Analysis," in IEEE Journal of Emerging and Selected Topics in Power Electronics, vol. 5, no. 4, pp. 1487-1498, Dec. 2017.

[8] X. Wang and F. Blaabjerg, "Harmonic Stability in Power Electronic Based Power Systems: Concept, Modeling, and Analysis" in IEEE Transactions on Smart Grid.

[9] W. Wu, Y. Liu, Y. He, H. S. H. Chung, M. Liserre, and F. Blaabjerg, "Damping methods for resonances caused by lcl-filter-based current-controlled grid-tied power inverters: An overview," IEEE Transactions on Industrial Electronics, vol. 64, no. 9, pp. 7402–7413, Sept 2017.

[10] P. Kundur, Power System Stability and Control. New York: McGrawHill, 1994.

[11] Z. X. Zou, G. Buticchi, and M. Liserre, "Analysis and stabilization of a smart transformer-fed grid," IEEE Transactions on Industrial Electronics, vol. 65, no. 2, pp. 1325–1335, Feb 2018.

[12] Franklin, Gene F., J. David Powell, and Michael L. Workman. Digital control of dynamic systems. Vol. 3. Menlo Park, CA: Addison-wesley, 1998.

[13] M. Belkhayat,"Stability criteria for ac power systems with regulated loads" Ph.D. dissertation, School Electr. Comput. Eng., Purdue Univ., Dec. 1997.

[14] J. Sun, "Small-signal methods for AC distributed power systems–A review" IEEE Trans. Power Electron., vol. 24, no. 11, pp. 2545–2554, Nov. 2009.

[15] Teodorescu Remus, Marco Liserre, and Pedro Rodriguez. Grid converters for photovoltaic and wind power systems. Vol. 29. John Wiley & Sons, 2011.

[16] Y. Wang, X. Wang, F. Blaabjerg and Z. Chen, "Harmonic Instability Assessment Using State-Space Modeling and Participation Analysis in Inverter-Fed Power Systems," in IEEE Transactions on Industrial Electronics, vol. 64, no. 1, pp. 806-816, Jan. 2017.

[17] J. Rocabert, A. Luna, F. Blaabjerg and P. Rodríguez, "Control of Power Converters in AC Microgrids," in IEEE Transactions on Power Electronics, vol. 27, no. 11, pp. 4734-4749, Nov. 2012.

[18] E. Wu and P. W. Lehn, "Digital Current Control of a Voltage Source Converter With Active Damping of LCL Resonance" in IEEE Transactions on Power Electronics, vol. 21, no. 5, pp. 1364-1373, Sept. 2006.